Stack Ventilation Within a Structural Spar: Development and Validation of a Natural-Ventilation Channel in a 70 m Carbon-Composite Mast

Dr. Bob van Someren, {Foundationº}
Edoardo Volpe, Carbo-Link

ABSTRACT: *This paper describes the engineering development and validation of a 70-metre one-piece carbon-composite mast incorporating an integrated passive ventilation system, the first of its kind in superyacht construction. Carbo-Link carried out the work for Sailing Yacht Zero, a vessel designed around full energy autonomy. Solar irradiance on the external mast surface generates a buoyancy-driven pressure differential sufficient to sustain continuous airflow along the full spar height, delivering ventilation power equivalent to 5–10 kW and meaningfully reducing mechanical air-conditioning demand. The central challenge was to embed the defined airflow channel geometry and inlet and outlet sizing within one of the main structures of the yacht's primary propulsion systems: the spars. The paper covers the full development sequence: feasibility modelling, channel design, prototype fabrication, and iterative validation of both ventilative and structural performance, with implications for passive energy management across high-performance vessel design and for mindset changes in spars design and structural engineering.*

1 Introduction

Energy efficiency is an important consideration in designing systems that reduce energy consumption and dependence on conventional energy sources. The SY Zero project explores various energy conservation and generation strategies within the design and construction of a superyacht. One essential requirement for any inhabited vessel is adequate climate control and ventilation. This paper investigates the potential to harness the natural stack effect within the hollow structure of a yacht's mast to facilitate passive airflow. By integrating ventilation requirements into the mast's structural design from the outset, the mast can fulfil a secondary function as an air conduit without compromising its primary structural purpose. This approach explores the potential of multifunctional structural design to reduce reliance on mechanically driven ventilation systems and, consequently, overall energy demand.

2 Ventilation by Stack Effect

2.1 Spars Designed for Ventilation of Living Quarters by the Stack Effect

The stack effect, commonly observed in chimneys, is driven by buoyancy resulting from a density difference between the air inside and outside a vertical conduit. In the mast ventilation concept presented here, this density difference is generated through solar heating of the air within the spar's central channel. As the internal air warms, its density decreases relative to the surrounding ambient air, creating an upward buoyancy-driven airflow. To facilitate this process, the spar was specifically designed with a sufficiently large, unobstructed central channel extending continuously from the mast foot to the masthead. Appropriately sized inlet and outlet openings were also incorporated to minimise flow restrictions and facilitate the required airflow. These ventilation features were integrated from the outset alongside the spar's primary structural requirements, with the objective of enabling passive airflow while maintaining structural integrity and load-bearing function.

2.2 Analysis of Solar Powered Stack Effect

The thermal energy driving the ventilation system originates from solar radiation absorbed by the dark external surface of the mast. This energy is transferred to the inside central channel by the thermal conductivity of the wall. This heat warms the inside air, which then expands and, through buoyancy, rises. As the Reynolds number of the channel, even at low flow velocities, is far greater than the turbulence limit, the flow is assumed to be turbulent in all conditions. Turbulent flow and higher flow velocity further increase energy exchange from the channel wall to the internal air through mixing. Warming the air requires heat because the heat capacity of air is about 1 kJ/m3/K, so as the flow rate increases, more heat is required to warm the larger mass of air flowing. Eventually, an equilibrium is reached where the energy required to sustain the air flow matches the available solar power. At the same time, the channel's flow resistance must be overcome by the buoyancy forcing the air upward. Matching these two forces, together with the heat-flow equilibrium described above, determines the eventual flow rate and the temperatures involved. In our analysis, we aim to show how these basic principles lead to mathematical expressions. Therefore, in order not to overcomplicate the equations, some reasonable simplifications are made. The justification is given where applicable.

The following physical principles determining the overall performance are:

1. The absorbance of the solar radiation by the outside surface of the spar
2. The heat transfer through the wall of the spar towards the flow channel inside the spar
3. The heat transferred from the channel wall to the air must equal the heat used to warm the air inside the spar channel. This is the heat equilibrium.
4. The buoyancy force of the lighter, heated air must equal the flow resistance of the spar channel plus the in- and outflow openings. This is the force equilibrium.

Together, the equations derived from 3 and 4 will be solved numerically to find the flow rate and the relevant temperatures.

We assume the overall efficiency of solar absorption is close to 100% because the spar is coloured black. We assume the effect of wind carrying away some energy from the spar surface is small, as we analyse low-wind-speed conditions. Furthermore, to estimate the solar flux, we assume the yacht is moored in Palma.

Point 1: The main spar is 70 meters tall and has an oval shape with an average diameter of 60 cm. We assume the total perpendicular surface of the spar exposed to the sun is 40 m2, and with a daily solar flux profile as shown in Figure 1, we can expect between ca. 5 kW and well over 25 kW of solar power available between 8 and 16 hours.

Point 2: The thermal conductivity perpendicular to the carbon fibres of the high-density carbon composite used for the spar is 1.5 W/m/K, which gives the on-average 10 mm thick wall a U value of 150 W/m2/K or a total heat conductivity of ca 10 kW/K. The temperature drop over the spar wall is thus in the range of 0.5 to 2.5 degrees. Since the temperature of the spar in full sun can reach 60-70 degrees, the thermal resistivity of the spar wall is insignificant in the heat transfer analysis. Instead, the thermal resistance of heat transfer from the inside wall to the inside air dominates.

Point 3: First, we need to determine how much heat can be transferred to the air from the inside

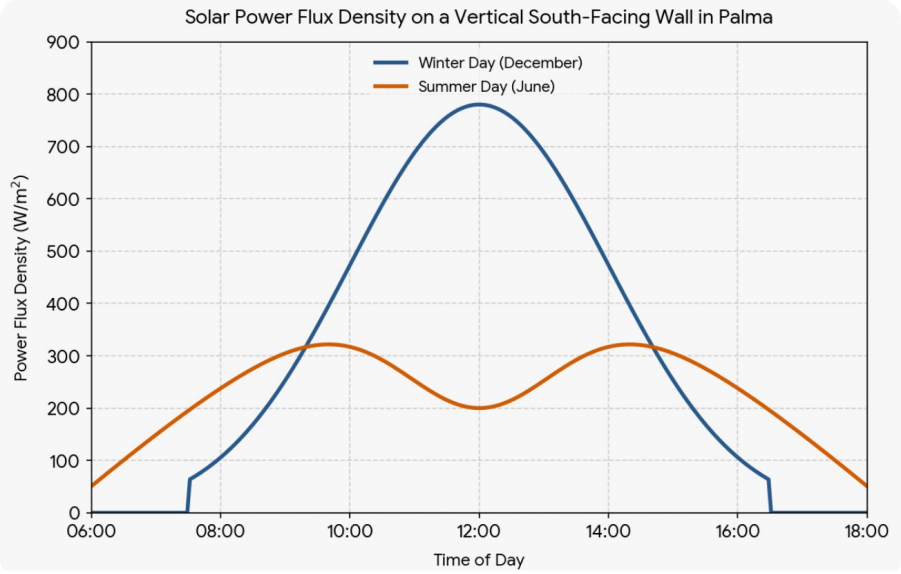


Figure 2- 1: Winter and summer solar flux on vertical surface in Palma de Mallorca (Spain)

wall of the channel. For this, we need to know whether the flow is laminar or turbulent and from that we derive the ratio of convective to conductive heat transfer for the air. For turbulent flow to occur, the Reynolds number should be larger than 10.000.

The Reynolds number for ca 60 °C air in a channel of 0.6 m diameter:

$$\Re(v) = 3.175.10^5 v \qquad \text{Equation 1}$$

where v is the flow velocity of the air. The turbulence condition in the channel holds for flows larger than ca 30 cm/sec, so we can assume the flow is always turbulent.

For simplicity, we assume that convection driven by the draft dominates buoyancy from heating in the natural boundary layer. In other words, heat exchange is a forced macro effect rather than a microscopic effect. With this simplification, the ratio of convective and conductive heat transfer for air is given according to the Dittus-Boelter equation by the Nusselt number:

$$Nu_f = 0.02.(\Re)^{0.8} \qquad Equation\ 2$$

Even at a moderate flow of 30 cm/s, the Nusselt number is 30, meaning ca. 97% of heat transfer occurs through turbulent mixing.

Using the Nusselt number, we calculate the heat transfer coefficient for heat transferred from the channel wall to air flowing through the 60 cm diameter channel at ca 60 °C from:

$$h(v) = Nu.\frac{k}{D} \approx 3.5\, v^{0.8}\, W/m^2/K \qquad Equation\ 3$$

We need this number to calculate the thermal power that is transferred to the air by the inside wall of the channel:

$$Q_{tr}(v, T_i) = h.A.\Delta T_{\ln} \approx 231\, v^{0.8} \Delta T_{\ln} \qquad Equation\ 4$$

Where

$$\Delta T_{\ln} = \frac{(T_{out} - T_{amb})}{\left(\ln\left(\frac{(T_{wall} - T_{amb})}{(T_{wall} - T_{out})}\right)\right)} \qquad Equation\ 5$$

Equation 5 is the log-mean temperature. The temperature difference between the air and the channel wall isn't the same everywhere. At the bottom, near the inlet, the temperature difference between the wall and the air is larger, so energy transfer is higher. At the masthead, the air is already warmed, and the temperature differential is smaller, resulting in lower energy transfer. To incorporate this effect in Equation 4, we introduce the log-mean temperature. Also, we assume half of the spar surface is heated by the sun, and T_{amb} is 30 °C.

The power given in Equation 4 has to be equal to the power required to heat the air, which is:

$$Q_{Cv}(v, T_i) = Av\rho C_p(T_{out} - T_{amb}) \approx 330\, v\,(T_{out} - T_{amb}) \qquad Equation\ 6$$

In equilibrium, these two Q values must be equal and equal to the available solar power. This gives us the first set of equations from which we solve the flow v and the respective temperatures T_{out} and T_{wall}.

However, to fully solve for (v, T_{out}, T_{wall}), we need another equation. These are the equations of point 4, the flow resistance force matched by the force of the buoyancy.

The buoyancy pressure of the heated and expanded air is:

$$P_B(T_i) = \rho g H \frac{(T_{av} - T_{amb})}{(T_{av})} \approx 800 \frac{(T_{out} - T_{amb})}{(T_{out} + T_{amb})} \qquad Equation\ 7$$

which has to be equal to the pressure needed to drive the airflow in the presence of the friction of the channel, which is equal to:

$$P_{fri}(v) = f(v)\frac{H}{D} 1/2\, \rho\, v^2 \qquad Equation\ 8$$

Where:

$$f(v) = (-1.8 \log_{10}[(\epsilon/(3.7\,D))^{1.11} + 6.9/\Re(v)])^{-2} \qquad Equation\ 9$$

and for simplicity, the wall roughness e is set to 3.7 mm.

The equations depend on the temperature variables T_{out}, T_{wall} and the flow velocity v.

The full set of equations is solved numerically in an iterative Newton-Raphson method. The airflow and temperatures for different input powers are tabulated below.

Power (kW)	Airflow(m/s)	Mass flow(kg/s)	Volume (m3/h)	Tout(C)	Twall(C)
5	2.1	0.7	2100	37	44
10	2.7	0.9	2700	42	54
15	3.1	1.0	3100	45	52

20	3.4	1.1	3400	48	69
25	3.7	1.2	3700	51	75

Table 2-1

These values are calculated assuming no input or output restriction. In practice, however, the spar is not open on both ends. We added **inlet** and **outlet** openings: 1,256 cm2 for input and 2,030 cm^2 for outflow. The restrictive effects are absorbed into the f factor in Equation 8, and the resulting impact on the performance can be seen by comparing Table 2-2**.**

Power (kW)	Airflow(m/s)	Mass flow(kg/s)	Volume (m3/h)	Tout(C)	Twall(C)
5	0.74	0.7	1600	39	51
10	0.94	0.9	2000	45	64
15	1.1	1.0	2300	50	76
20	1.18	1.1	2500	54	87
25	1.28	1.2	2800	58	97

Table 2-2

3 Spar product adaptation, from technical debt to new opportunities

The first optimisation target for large yacht and performance sailing boat masts is traditionally weight. The light spars package increases safety, comfort and performance. For SY Zero, we set an additional target: optimize the mast's internal space for airflow. Previously, the mast bore was considered only as residual space for structural reinforcements and systems, but in this project it became a critical tool for a successful semi-passive ventilation system for the entire vessel. Together with the internal unconstructed space, other new points of attention raised from the classical design are listed in Table 3-1.

	TRADITIONAL PRINCIPLE	WHAT THE VENTILATION DUTY DEMANDS	PRIORITY
I	The Mast bore is a residual space	*A specified flow channel, continuous heel to head*	MUST
II	Top and bottom aperture maximised	*Two large apertures in region carrying peak compression*	MUST
III	Solar soak is a compliance check	*The wall is a deliberate absorber at 51–80 °C, sustained, daily, under load*	MUST
IV	Section sized for buckling and bending at minimum mass and maximum bore	*Inner mould line became a point of attention to maximise flow*	OPT
V	Internal finish is cosmetically irrelevant	*Roughness enters the friction term and sets the flow rate*	OPT
VI	Rig design follows the general arrangement	*Channel, apertures and reinforcement must freeze together*	MUST

Table 3-1: Shift of attention in mast design

To tackle Point I of the table, all possible fittings which transfer external loads to the mast tube, such as forestay tangs, running backstays, check stays, have been reduced to metal fittings bearing and pulling on the mast section surface, without the use of any traditional bullheads/brackets (Figure 3-1). Section 4.2 presents a case study of the running backstay design.

Points III and V were addressed by improving classical production methods. Using proprietary prepregs, we cured the mast tubes to temperatures up to 120 °C, increasing the delta above the expected 80 °C in operation. To improve internal surface finish, we used silicon vacuum bagging in combination with 6 bars of applied pressure during curing.

Point IV was achieved by developing a new geometry based on the interaction between a particular closed thin wall and internal Omega Stiffeners. To validate this approach, a stability test was carried out at EMPA (Swiss Federal Laboratories for Materials Science and Technology) during structural feasibility study 4.1.

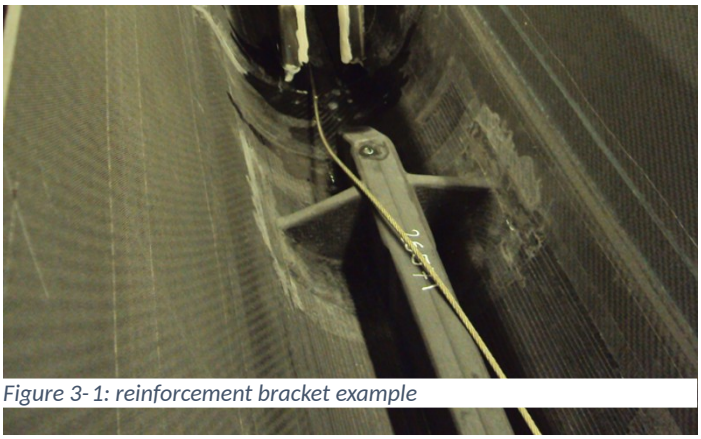


Figure 3-1: reinforcement bracket example

Points II and VII have been addressed through close coordination between adiabatic flow implementation and mast operability and maintenance.

4 Structural Validation, case study of Tube Wall Buckling and Runner Fitting.

For class approval, all spar structures for SY Zero had to meet the following criteria:

CRITERION	SAILING (W1)	SURVIVAL /EXTREME (W2)
Global laminate strain	< 0.25%	< 0.33%
Laminate at cut-outs	Stress factor 0.25 on material data	0.33
Metal load-introduction parts	Stress factor 0.65	
Stability – global, panel and thin wall	RF ≥ 3.0	RF ≥ 3.0

Table 4-1

The criteria in Table 4-1 are applied through three linked checks: a global stability check against shell buckling, a ply-level fibre and inter-fibre failure check on the laminate, and a stress check on the metallic load-introduction parts. The equations below make each check explicit and show how the reserve factors quoted in sections 4.2 and 4.3 were obtained.

4.1 Supporting Theory

For an axially loaded thin, closed cylindrical shell, the classical, imperfection-free buckling stress follows the Lorenz–Timoshenko solution, Equation 10, where E is the axial modulus of the wall, the wall thickness and R the shell radius. For an orthotropic laminate, E is taken as the effective axial modulus of the laminate stack. This is the value of a force-controlled linear eigenvalue solution, such as the 1200 kN result quoted in section 4.2, that converges for a defect-free model of the same geometry.

$$\sigma_{cl} = Et/R\sqrt{3(1-\nu^2)} \approx 0.605\,Et/R\,(\nu = 0.3) \qquad \textit{Equation 10}$$

Real shells buckle well below this value because manufacturing and geometrical imperfections trigger the shell's post-buckling instability at a much lower load. Since the 1930s, this has been captured empirically rather than predicted from first principles; the design curve retained in this study is the lower-bound knockdown factor from NASA SP-8007 (NASA, 1968), Equation 11 and Equation 12, where φ depends only on the section's radius-to-thickness ratio.

$$\varphi = 1/16\sqrt{R/t} \qquad \textit{Equation 11}$$

$$\gamma = 1 - 0.901\,(1 - e^{-\varphi}) \qquad \textit{Equation 12}$$

For the mast section R/t, this returns a knockdown γ ≈ 0.6, matching the "approximately 0.6" lower-bound figure used in section 4.2 to judge the measured 58 % result. The design buckling resistance and the reserve factor reported throughout the paper follow directly,

Laminate strength at cut-outs and load-introduction points is checked ply-by-ply against Puck's fibre-failure (FF) and inter-fibre-failure (IFF) criteria (Puck and Schürmann, 2002), as implemented in ACP Post. Fibre failure is a maximum-stress check on the fibre-direction stress σ1 against the tensile and compressive fibre strengths Xt and Xc, Equation 14.

$$f_{E,FF} = \sigma_1/X_t\,(\sigma 1 \geq 0) - \sigma_1/X_c\,(\sigma 1 < 0) \qquad \textit{Equation 14}$$

Inter-fibre failure is evaluated on the action plane that maximises the stress exposure, combining the transverse stress σ2 and the in-plane shear τ21 acting on that ply. For the tensile transverse mode (Mode A, σ2 ≥ 0), the stress exposure factor is given by Equation 15, where S21 and S2t are the in-plane shear and transverse tensile strengths, and $p_{\perp\parallel}$ is the mode inclination parameter (taken as 0.3 for the carbon/epoxy system used here, per Puck and Schürmann, 2002). A ply is safe while $f_e \leq 1$; the inverse reserve factor quoted in 4.3, peaking at 1.22 at the port runner cut-out, is this exposure factor read directly from the ply-by-ply ACP Post output.

$$f_{E,IFF} = \sqrt{(\tau_{21}/S_{21})^2 + (1 - p_{\perp\parallel} S_{2t}/S_{21})^2 (\sigma_2/S_{2t})^2} + p_{\perp\parallel}\,\sigma_2/S_{21}\,(Mode\,A, \sigma 2 \geq 0) \qquad \textit{Equation 15}$$

Because f_e is evaluated on discrete plies at a modelled cut-out edge, a local peak driven by the mesh or the laminate drop-off idealisation is expected, and is judged, as in section 4.3, against the governing physical failure mode, here bearing stress at the fitting, rather than in isolation.

4.2 Large section thin wall buckling validation

To validate the approach of a larger thin-walled mast section at the beginning of the product development campaign, a full-scale half-mast section under compression was tested at EMPA.

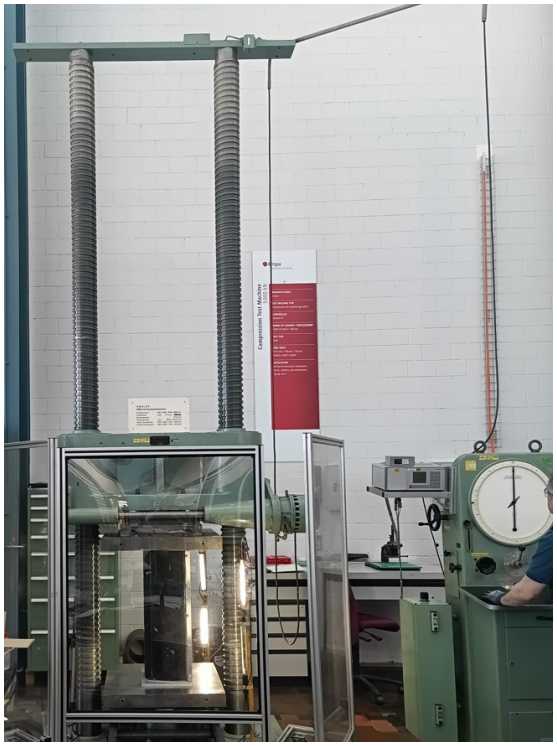


Figure 4- 1: Compression test set up at EMPA

The mast segment was tested to destruction in compression on a 5000 kN testing machine, in two successive runs on the same specimen. Composite aluminium angles were bonded along the vertical edges and rotation was restrained at both ends, matching the boundary conditions of the finite-element model against which the result is compared. That model contains neither geometric imperfections nor pre-damage, and predicts first buckling at approximately 1200 kN when solved as a force-controlled linear eigenvalue problem and at approximately 900 kN in a displacement-controlled non-linear solution. In the first run, the first buckle pattern became visible at approximately 700 kN, observed as a break in the specular highlight running down the panel. At approximately 850 kN, a second pattern appeared abruptly on one side; the force trace flattened at this point, but the machine was regulated by hand on oil flow, and the change of slope is therefore not by itself evidence of a loss of stiffness. Loading continued to a peak of approximately 1073 kN, at which an audible failure occurred and the load fell briefly to about 1040 kN before recovering; damage to the lower corner, the end restraint, and the laminate was observed. In the second run, carried out on the now-damaged specimen, no global buckling occurred: the softened lower corner kinked locally, and the specimen then failed in compression across one half of the section at 937 kN, collapsing to below 120 kN within a quarter of a second.

The measured onset of buckling is 58 % of the idealised force-controlled prediction and 78 % of the displacement-controlled one. Compared with the literature, published lower-bound knockdown factors for cylindrical shells with initial geometric imperfections are about 0.6 in the thickness ratio range of this section, so a measured 58 % against an imperfection-free eigenvalue numerical calculation reflects a model behaving exactly as the accumulated experimental results show.

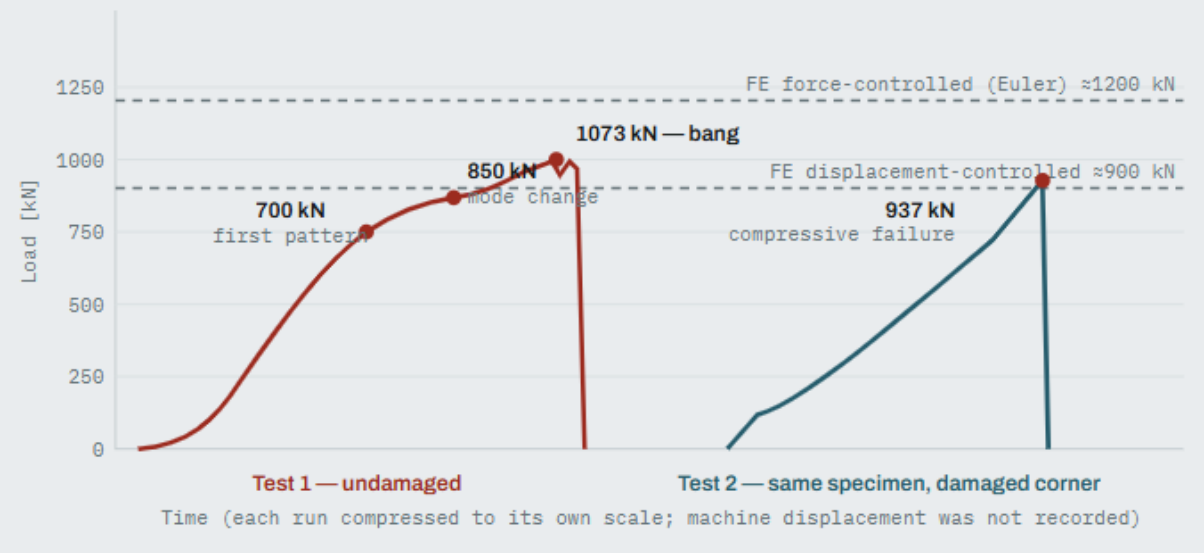


Figure 4-2: Stability test summary graphs

The practical consequence is a margin, not a correction. With a required reserve factor of 3.0 applied to the Euler calculation, the residual margin against first buckling after the measured knockdown is 1.74, or 1.8 if the published lower bound is used in place of the measured value. Two further observations bear on how to interpret that margin. First, the first buckle is not a collapse mechanism in this structure: the specimen carried load from approximately 700 kN through 850 kN and beyond 1020 kN before anything broke, and the displacement-controlled solution shows the same behaviour, with capacity continuing past first buckling at only slightly reduced stiffness. Second, both runs ended at the same lower corner, indicating damage tolerance at edges and discontinuities rather than panel stability in the shell field.

.

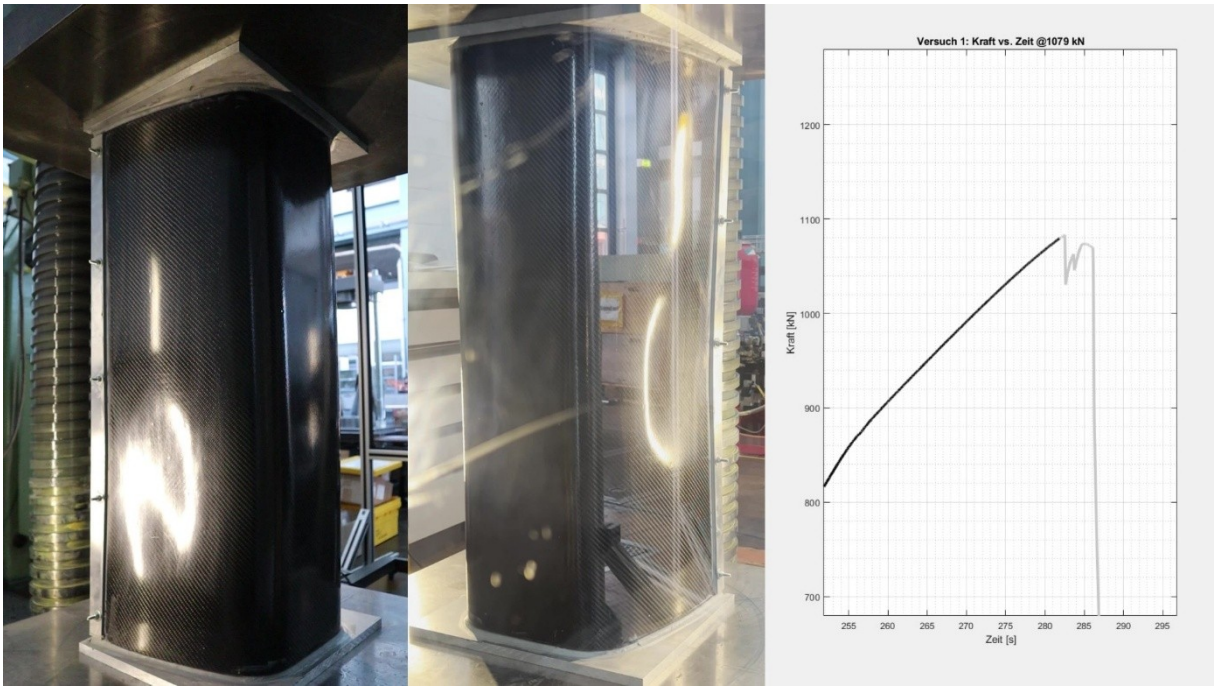


Figure 4-3: Mast segment in the testing machine at 1073 kN, immediately before failure. The buckle lobe is visible in the reflected highlight; the trace at right shows the load dip at the failure event.

On that basis, the reserve factor of 3.0 on Euler calculations usually required by Spar maker classification society was retained as valid for more unconventional, aggressive thin-walled spar sections.

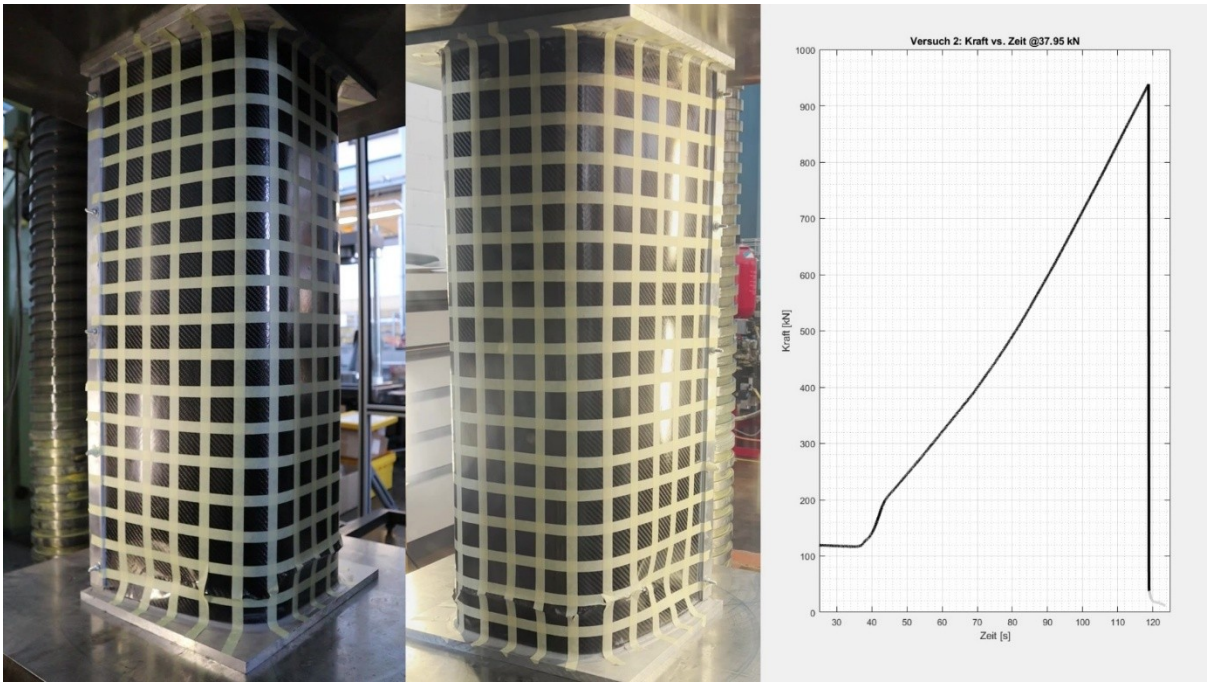


Figure 4-4: Mast half-Section after collapse on second test

4.3 Case study: Runner tang and mast head designed with Stack Ventilation in mind

Rig engineers reacting to an eccentric tang load of this magnitude have four conventional options, and the ventilation duty removes or constrains each of them.

An internal compression strut or tie-tube spanning the section diametrically converts the point load into a reacted couple carried largely as shell compression, but any diametral member blocks the duct outright and fails the requirement for an unobstructed bore from foot to head. A ring frame or diaphragm at the load station preserves local roundness and distributes the load into hoop stress, but closes the bore completely and is incompatible with a flow-through duct by definition (section on the left of Figure 4-7).

The only route is to build a local build-up of the wall itself, which meets the product functionality constraint, but only if the build-up grows inward as laminate rather than inward as structure, so the change in bore geometry is a gradual thickness transition rather than a step. In the design phase, the high out-of-plane loads at the spreader and tang connection did not allow us to move away from connecting the tow faces of the mast section, but for the aft rigging connection we had the opportunity to increase the internal bore section.

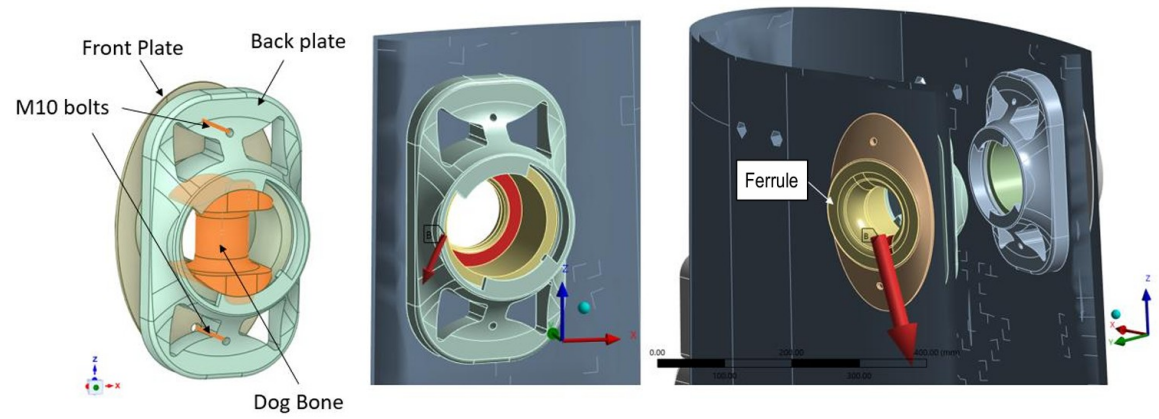


Figure 4-5: Runner parts, loading and position in the mast

The evaluation was carried out in ANSYS Workbench, with the lay-up in ACP Pre and ply-by-ply assessment in ACP Post, against Puck's failure criterion.

The results are based on a line load of 253.6 kN on W1 and 288.9 kN on W2 and showed a structurally sound design with an incremented “suction” area by about 17.5% in comparison to the traditional layout.

On the laminate, the Puck inverse reserve factor at the port runner cut-out peaks at 1.22; at the critical sampling point, only three plies exceed 1. Judged safe against a bearing stress that is 17 % of the 233 MPa permissible.

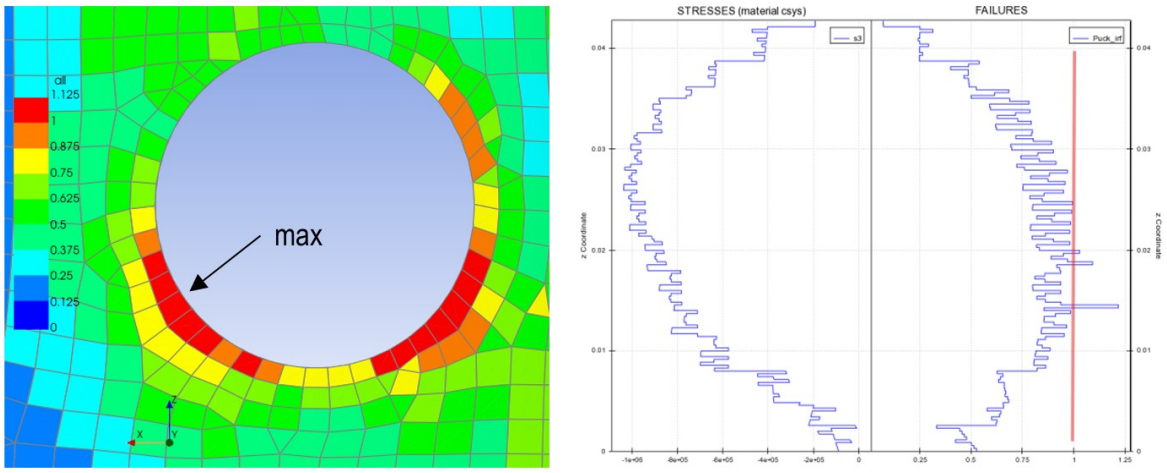


Figure 4-6: Inverse reserve factor of runner cutout

On the metal front plate at 52 % and the back plate at 69 % of the 540 MPa permissible for Ti-6Al-4V Grade 5; the super-duplex ferrule touches 103 % of 358 MPa at a single point, attributed to numerical inaccuracy. The dogbone showed 116 MPa bearing against 293 MPa permissible, safety factor 2.5.

In stability, nonlinear buckling at the mast head gives a minimum load multiplier of **3.5** for the runner-and-forestay case (LC4, W1) and 6.6 for full-hoist-and-forestay (LC2, W1), both above the required 3.0. Buckling initiates at the bottom of the modelled segment where the wall is thinnest, i.e. away from the patched tang.

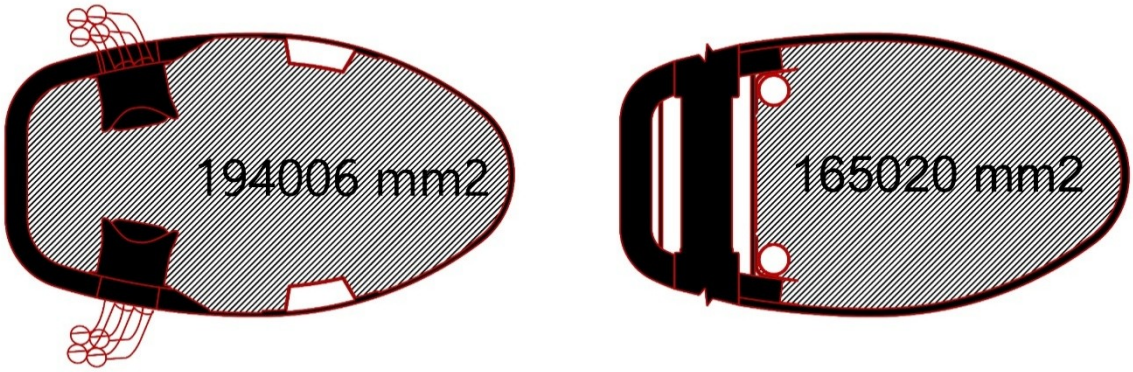


Figure 4-7: Comparison of ventilation area between traditional vs. optimized runner fittings on the Sy Zero Main mast taper

5 Conclusions

This paper has shown that a superyacht's primary structure, the mast, can be made to carry a second, independent function, passive ventilation of the accommodation, without giving up its first function as a loaded lightweight spar, provided the ventilation duty is treated as a design driver from the earliest concept stage rather than retrofitted.

Solar heating of the outer laminate alone is sufficient to drive a continuous stack-effect airflow through the hollow core of the SY Zero main mast: modelled flow rates run from about 1600 m^3/h at 5 kW of available solar power to about 2800 m^3/h at 25 kW once the real inlet and outlet openings are accounted for, with channel-wall temperatures rising from roughly 51 °C to the high nineties across that range. No fan or other active component is required to obtain this airflow. Delivering that airflow required the mast bore to shift from residual space around the structure to a specified flow channel, unobstructed from foot to head, with entrance and exit openings sized for flow rather than convenience.

Every fitting that historically reacted external loads through internal bulkheads or brackets, such as forestay tang, running backstays, or checkstays, was instead reduced to a metal fitting bearing directly on the mast tube surface, and any local increase in wall thickness needed to carry those loads was accommodated as a gradual laminate build-up rather than a step into the bore. This is the practical answer to what would otherwise be a direct conflict between structure and ventilation.

The running backstay case study carried this from principle to a built detail. With the internal strut, tie-tube, and diaphragm options excluded by the requirement for a clear bore, the load path was resolved entirely within the laminate: a local, tapered wall build-up under the fitting, verified ply-by-ply against Puck's failure criteria and checked in the surrounding metalwork against yield and bearing allowable. The laminate Puck inverse reserve factor peaks at 1.22 on three plies at the cut-out edge, judged acceptable against a governing bearing stress of only 17 % of allowable; the metal fittings run at 52–69 % of their permissible stress, with one local reading at 103 % attributed to a numerical artefact at a single node and flagged here for confirmation rather than treated as closed.

Global stability under the same load case returns load multipliers of 3.5 and 6.6 against the required 3.0, with the critical mode initiating away from the reinforced fitting, indicating that the local reinforcement does not simply relocate the weak point elsewhere in the section.

The optimised fitting also increased the usable ventilation area at this station by about 17.5 % relative to a traditional internal-strut layout, so the same design change that solved the structural problem improved the ventilation performance it was meant to serve.

Validation of the stability reserve factor of thin-wall sections, performed via a full-scale half-mast section loaded to destruction at EMPA, supported the choice to increase the mast section and reduce wall thickness using local stiffeners. The specimen buckled at about 58 % of the force-controlled linear eigenvalue prediction and about 78 % of the displacement-controlled non-linear prediction; a result that sits squarely inside the published lower-bound knockdown band ($\gamma \approx 0.6$, Equations 11–12) for cylindrical shells of this thickness ratio. Applied against the required reserve factor of 3.0 on the classical Euler stress, this leaves a residual margin of 1.74–1.8 after the empirical knockdown is applied, confirming that the standard RF = 3.0-on-Euler design rule used by spar classification societies remains valid for this larger, thinner, and deliberately more open section, without the need for a bespoke margin

More generally, the method demonstrated in this paper treats the secondary function as a structural design driver at the same design stage as the primary one, and resolves any resulting conflict by building load capacity into the wall rather than across the enclosed volume; this is not specific to masts or ventilation. It applies to any primary structure whose internal volume is currently treated as dead space, and it is offered here as a transferable design rule for that broader class of problem, not only as a description of one spar. That approach was tested, not just modelled.

ACKNOWLEDGEMENTS

The authors acknowledge Andre Guerotto, Michael Dreyer, and Congzhe Wang for the work done on the Stability test and FEA, EMPA (Swiss Federal Laboratories for Materials Science and Technology) for their support during the stability test, SY Zero, {Foundation°} and Carbo-Link AG for the possibility of sharing the results in this paper.

REFERENCES

1. NASA (1968). Buckling of thin-walled circular cylinders. NASA Space Vehicle Design Criteria, SP-8007. Source of the lower-bound knockdown factor applied in section 4.1 (Equations 11–12) and used to judge the section 4.2 EMPA result.
2. Puck, A. and Schürmann, H. (2002). Failure analysis of FRP laminates by means of physically based phenomenological models. Composites Science and Technology, 62(12–13), 1633–1662.